SBS suppression using PRBS phase modulation with different orders

J. T. YOUNG,[1,*] C. R. MENYUK,[2] AND J. HU[1]

[1] *Baylor University, One Bear Place, Waco, TX 76798, USA*
[2] *University of Maryland Baltimore County, 1000 Hilltop Circle, Baltimore, MD 21270, USA*
*joshua_young@baylor.edu

Abstract: The Brillouin instability (BI) caused by stimulated Brillouin scattering (SBS) can limit the output power of high-energy laser amplifiers. Pseudo-random bitstream (PRBS) phase modulation is an effective modulation technique to suppress BI. In this paper, we study the impact of the PRBS order and modulation frequency on the BI threshold for different Brillouin linewidths. PRBS phase modulation with a higher order will break the power into a larger number of frequency tones with a lower maximum power in each tone, leading to a higher BI threshold and a smaller tone spacing. However, the BI threshold may saturate when the tone spacing in the power spectra approaches the Brillouin linewidth. For a given Brillouin linewidth, our results allow us to determine the order of PRBS beyond which there is no further improvement in the threshold. When a specific threshold power is desired, the minimum PRBS order required decreases as the Brillouin linewidth increases. When the PRBS order is too large, the BI threshold deteriorates, and this deterioration occurs at smaller PRBS orders as the Brillouin linewidth increases. We investigate the dependence of the optimal PRBS order on the averaging time and fiber length, and we did not find a significant dependence. We also derive a simple equation that relates the BI threshold for different PRBS orders. Hence, the increase in BI threshold using an arbitrary order PRBS phase modulation may be predicted using the BI threshold from a lower PRBS order, which is computationally less time-consuming to compute.

1. Introduction

High-energy fiber amplifiers are becoming widely used in high-energy laser systems due to their high output powers and beam quality [1–3]. Nonlinear effects due to the high pump power often limit the output power. Typical nonlinear effects encountered with fiber amplifiers are the Brillouin instability (BI) [4–7] and the transverse mode instability (TMI) [2,7–11]. BI dominates in fiber amplifiers with a small core diameter since the incident light intensity increases as the core size decreases. Although using a larger core size will reduce the impact of BI, it may increase the number of modes in the core and lead to TMI [7,12,13].

Techniques for BI suppression that have been proposed include reducing the overlap between optical and acoustic modes [14], laser gain competition [15], and phase modulation [16–20]. The latter has been successfully used to suppress BI without changing the fiber design [16–24]. When laser light passes through an optical fiber, each component in the laser spectrum will have a Brillouin gain linewidth associated with it, which is typically redshifted by an amount ranging from 11 GHz to 32 GHz [25–27]. Phase modulation of the input light source works by broadening the laser linewidth so that it is larger than the Brillouin gain linewidth, lowering the peak Brillouin gain, and equalizing the gain across the entire spectrum. Proposed phase modulation techniques include white noise [19,21], sinusoidal [19], chirped seed [24], piecewise parabolic phase [28], and pseudo-random bitstream (PRBS) [19–23]. Among these techniques, PRBS phase modulation has been proved in both experiments and simulations to be an effective technique to suppress BI [19–23]. In this paper, we computationally study PRBS phase modulation with different orders. We calculate the relationship between the threshold and Brillouin linewidth

as the PRBS order increases. With a larger PRBS order, the total power is spread across more tones with a lower maximum power in each tone, which decreases the peak Brillouin gain and reflectivity for a given linewidth. As the order increases, the decrease in reflectivity at a fixed modulation frequency will eventually saturate when the frequency tone spacing approaches the Brillouin linewidth. We define reflectivity as the ratio of average reflected Stokes power at the input side of the fiber to the input power. Further increasing the PRBS order will not further decrease the reflectivity since the total power within the Brillouin linewidth is almost the same. We also study enhancement with different fiber lengths and averaging time. We later derive a simple equation that relates the BI threshold for different PRBS orders, which can be used as a computationally time-efficient method to predict the threshold increase with an increased order. New lithium niobate electronics have an increased phase modulation bandwidth [29], and we anticipate that our analysis will be useful in the selection of PRBS parameters that produce optimal performance.

In many cases, the finite bandwidth of the electronics generating the PRBS signal and the limitations of the electro-optic modulators impose penalties on the fidelity of the phase modulation [30]. Some prior studies have demonstrated the impact of non-ideal PRBS modulation through the use of a low pass filter [31]. In those cases, our study yields an ideal limit that gives guidelines for the optimal PRBS order and modulation frequency.

2. PRBS modulation scheme and SBS model

An all-fiber Yb-doped fiber amplifier is commonly used for the experimental investigation of laser power scaling via PRBS phase-modulated signals. A seed laser operating at 1064 nm is often used [20,22,23]. A PRBS generator and a lithium niobate (LiNbO3) electro-optic phase modulator driven by a radio-frequency (RF) source are placed between the seed laser and the fiber amplifier to broaden the linewidth of the seed laser. The electro-optic phase modulator is driven at the appropriate voltage to generate the '0' and 'π' binary phase shifts.

PRBS phase modulation consists of a maximum length pseudo-random bit sequence of length $2^N - 1$, where N is the PRBS order [19–23,32–34]. Maximum length sequences are commonly created using linear feedback shift registers (LFSRs) [32], where the order of the sequence equals the number of registers in the LFSR. Maximum length sequences are unique in the sense that they reproduce every possible sequence that can be represented by the registers in the LFSR used to create it. The duration of each bit in the time domain is equal to the inverse of the modulation frequency. Figure 1 shows an example of the phase for PRBS order 3 and PRBS order 5 using solid blue and dashed red lines with modulation frequencies of 1.0 and 4.4 GHz, respectively. These modulation frequencies were chosen so that the period of the entire bit sequence for both PRBS orders is the same. The PRBS orders 3 and 5 have $2^3 - 1$ and $2^5 - 1$ bits, respectively, in their sequences.

We now study the spectra associated with PRBS phase. Figures 2(a) and 2(b) show an illustration of the spectral content on a logarithmic scale for PRBS phase modulation with orders 3 and 5, respectively. The modulation frequency is selected such that both spectra have the same frequency tone spacing Δf, which is given by, $\Delta f = f/(2^N - 1)$, where f is the modulation frequency and Δf is the inverse of the period for the entire bit sequence in time domain. If one uses the same CW signal before phase modulation, the ratio of magnitudes of the peak power in the spectra in Figs. 2(a) and 2(b) will be 3.7:1. Since the majority of the power is distributed among different tones, the maximum power among all frequency tones, P_{max}, will be much lower than the total power, P.

We then study the BI for different PRBS orders. We use the coupled partial differential equations to model BI [4,19,35],
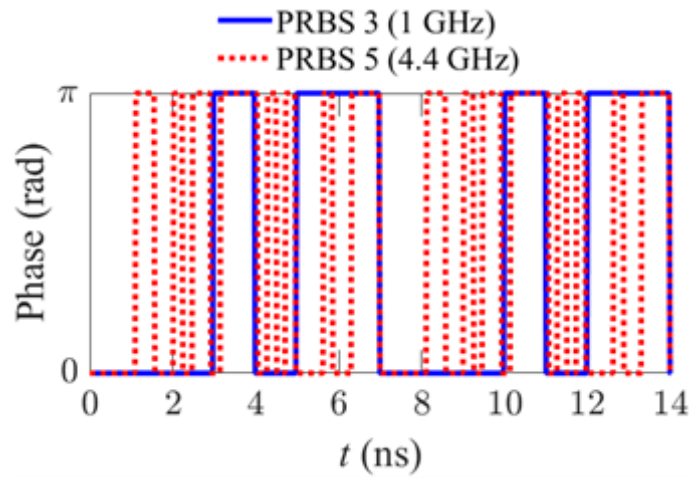
Fig. 1. Phase for PRBS 3 and PRBS 5 as a function of time.
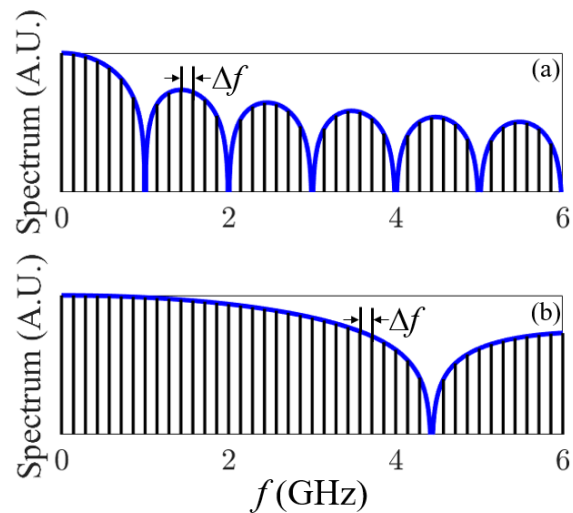
Fig. 2. Illustration of the spectra (a) for a PRBS signal of order 3 with a modulation frequency of 1.0 GHz and (b) for a PRBS order signal of 5 with a modulation frequency of 4.4 GHz. At the modulation frequencies of 1.0 and 4.4 GHz, the frequency tone spacing for the PRBS 3 and PRBS 5 signals are the same. The solid blue curves mark the characteristic sinc^2 envelope of the PRBS phase modulation, and vertical black lines mark the tones within the PRBS spectra.

$$\frac{\partial E_L}{\partial z} + \frac{n}{c}\frac{\partial E_L}{\partial t} = i\kappa E_S\rho, \tag{1a}$$

$$-\frac{\partial E_S}{\partial z} + \frac{n}{c}\frac{\partial E_S}{\partial t} = i\kappa E_L\rho^*, \tag{1b}$$

$$\frac{\partial \rho}{\partial t} + \pi\Delta\nu_B\rho = i\Lambda E_L E_S^* + f_n, \tag{1c}$$

where E_L is the forward propagating laser electric field, E_S is the backward propagating Stokes electric field, ρ is the acoustic density, κ is the optical coupling parameter, Λ is the acoustic coupling parameter, and $\Delta\nu_B$ is the Brillouin linewidth. The quantity f_n is the acoustic noise source where $\langle f_n(z,t)f_n^*(z',t')\rangle = Q(z-z')\delta(t-t')$ and Q is the phonon strength parameter [4]. Parameters for the simulation are given in Table 1. We use a relaxation algorithm to solve Eq. (1) for the BI. We first propagate the field E_L, and we then propagate the Stokes field E_S in the backward direction. The forward laser electric field is specified at the input side as $E_L(z=0) = 2P/(nc\epsilon_0 A)^{1/2}$, where P is the input power, n is the core refractive index, and A is the effective modal area. The backward Stokes electric field is specified at the output side as $E_S(z=L) = 0$. We first run the simulation for 40 transient fiber times, $t_f = Ln/c$, and we then average the reflected Stokes power at the beginning of the fiber for 40 more transient fiber times. Averaging the Stokes power using times greater than 40 transient fiber times does not significantly change results [4,24]. We discretize the fiber in the longitudinal direction using 1000 points. We verified that increasing the relaxation time, averaging time, and longitudinal discretization does not change our results. This sort of relaxation algorithm is commonly used for two-point boundary value problems [36].

Table 1. Simulation parameters

Fiber length	L	9 m	Electrostrictive constant	γ	1.95
Wavelength	λ	1064 nm	Core refractive index	n	1.45
Silica density	ρ_0	2201 kg/m^3	Effective modal area	A_{eff}	78.5 μm^2
Sound velocity	ν	5900 m/s	Temperature	T	300 K

3. Phonon lifetime and Brillouin linewidth

We first study how the reflectivity at the front of the fiber changes as a function of the Brillouin linewidth, which is related to the phonon lifetime, τ, by $\Delta\nu_B = 1/(2\pi\tau)$. Figure 3 shows reflectivity as a function of the Brillouin bandwidth or phonon lifetime with different PRBS orders. The phonon lifetime is a property of the glass material and depends on wavelength. As an example, to illustrate the reflectivity, we set the modulation frequency equal to 5 GHz in this section. Different modulation frequencies will also lead to the same conclusion.

We set the power equal to 16 W, which is the threshold power when the PRBS order is 3, the modulation frequency is 5 GHz, and the Brillouin linewidth is 57 MHz. This linewidth is in the typical range of linewidths for silica fibers [19,25–28]. We define the threshold power as the input power at which the averaged reflectivity reaches 1%. When the Brillouin bandwidth increases, the phonon lifetime and peak Brillouin gain both decrease, so that the gain is spread across more frequency components. Hence, a wider Brillouin bandwidth leads to a lower reflectivity. When the Brillouin bandwidth is between 10 to 100 MHz, results from Fig. 3 show that increasing the PRBS order while keeping the Brillouin linewidth the same will decrease the reflectivity. With a larger PRBS order, the total power is spread across more tones with a lower P_{max}, which decreases the peak Brillouin gain for a given linewidth. This decrease in reflectivity will eventually saturate when the frequency tone spacing, Δf, becomes smaller than the Brillouin linewidth. Beyond
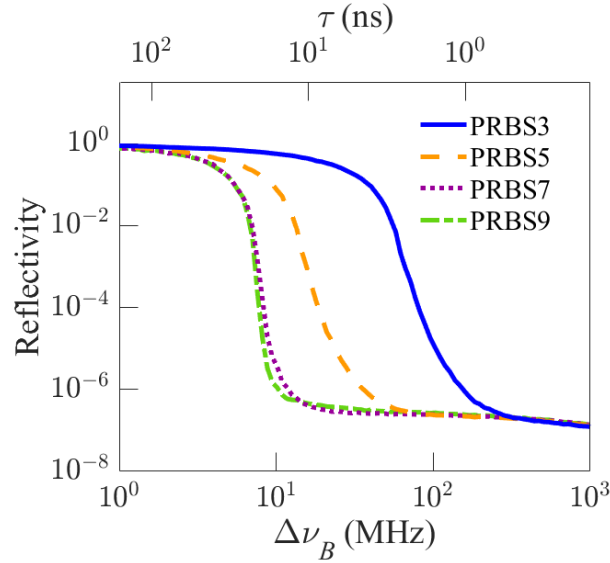
Fig. 3. Reflectivity as a function of the Brillouin linewidth or phonon lifetime for different PRBS orders.

a transition region as $\Delta\nu_B$ increases, increasing the PRBS order will not further decrease the reflectivity.

Table 2 shows the tone spacing, Δf, for different PRBS orders with a modulation frequency of 5 GHz. When Δf becomes roughly equal to $\Delta\nu_B$, saturation occurs. The reason is that further increasing the PRBS order does not lower the power within one Brillouin linewidth and thus does not decrease the Brillouin gain. The values in Table 2 correspond to the transition regions in Fig. 3. Comparing the values of Δf in Table 2 with Fig. 3, we see that the reflectivity when $\Delta\nu_B = \Delta f$ is close to the endpoint of the transition region as $\Delta\nu_B$ increases.

Table 2. Tone spacing for different PRBS orders with a modulation frequency of 5 GHz

PRBS Order	3	4	5	7	9
Δf (MHz)	714.3	333.3	161.3	39.4	9.8

Next, we study how the BI threshold changes as a function of the Brillouin linewidth for different PRBS orders. Figure 4 shows the BI threshold, P_{TH}, as a function of the Brillouin linewidth, $\Delta\nu_B$ or τ, using PRBS phase modulation with different orders. For every $\Delta\nu_B$, there is a PRBS order beyond which increasing the order leads to no further increase in P_{TH}.

The previous analysis shows that both the Brillouin linewidth and PRBS order contribute to the BI threshold. In Fig. 5, we show a contour plot of P_{TH} as a function of $\Delta\nu_B$ and the PRBS order. From Fig. 5, it is possible to find the minimum PRBS order for a specific power and a specific Brillouin linewidth. The black curve superimposed on Fig. 5 shows the transition point when the tone spacing Δf equals the Brillouin linewidth $\Delta\nu_B$. The region under the black curve corresponds to Brillouin linewidths that are less than Δf, and the region above the black curve corresponds to Brillouin linewidths greater than Δf. As the Brillouin linewidth increases, the minimum PRBS that can yield a given power threshold decreases. Conversely, the BI threshold begins to deteriorate at smaller PRBS orders as the Brillouin linewidth increases.
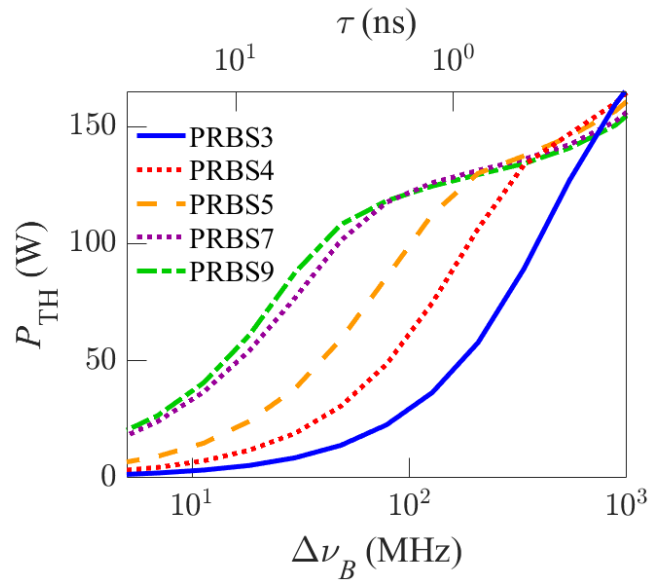
Fig. 4. BI threshold power, P_{TH}, as a function of the Brillouin linewidth or phonon lifetime.
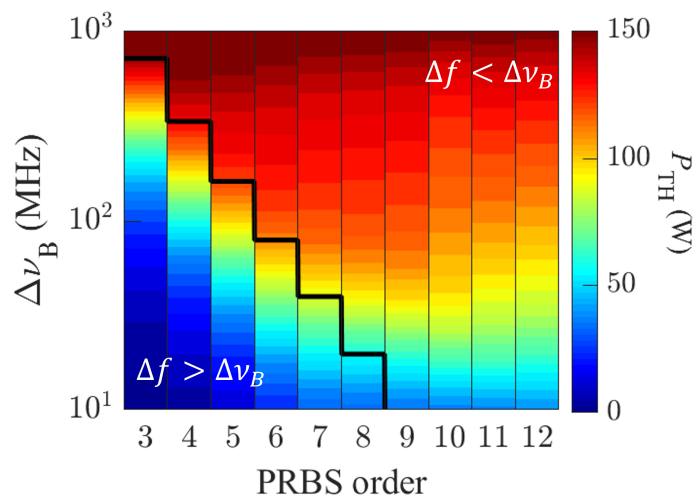
Fig. 5. BI threshold, P_{TH}, as a function of the PRBS order and Brillouin linewidth.

4. Enhancement as a function of PRBS order and modulation frequency

Different experiments use different PRBS orders and tone spacings. Hence, we consider multiple PRBS orders and tone spacings. We now study the impact of the PRBS order and modulation frequency on the BI threshold. We set the Brillouin linewidth to 57 MHz which is in the typical range for silica fibers [19,25–28]. Figure 6(a) shows the tone spacing, Δf, as a function of PRBS order and modulation frequency using $\Delta f = f/(2^N - 1)$. The solid black curve in Fig. 6(a) marks the frequency as a function of PRBS order when the tone spacing equals a Brillouin linewidth of 57 MHz in our simulation. Figure 6(b) shows the enhancement of the BI threshold relative to the unmodulated threshold as a function of PRBS order and modulation frequency. The solid black curve in Fig. 6(b) again illustrates the condition when the tone spacing Δf is 57 MHz. In Fig. 6(b), when operating above the solid black curve, the tone spacing Δf is larger than the Brillouin linewidth. Further increasing the modulation frequency and tone spacing with a fixed PRBS order will not significantly increase the BI threshold. On the right side of the black curve in Fig. 6(b), the tone spacing Δf is smaller than the Brillouin linewidth, and further increasing the PRBS order while keeping the modulation frequency constant will not significantly decrease the amount of power within the Brillouin linewidth to effectively increase the BI threshold. Hence, when Δf approaches the Brillouin linewidth, as indicated by the black curve in Fig. 6(b), simply increasing the modulation frequency or the PRBS order alone does not lower the Brillouin gain and will not significantly increase the enhancement. Of course, a higher enhancement can be achieved by increasing both the modulation frequency and PRBS order, as shown in Fig. 6(b).
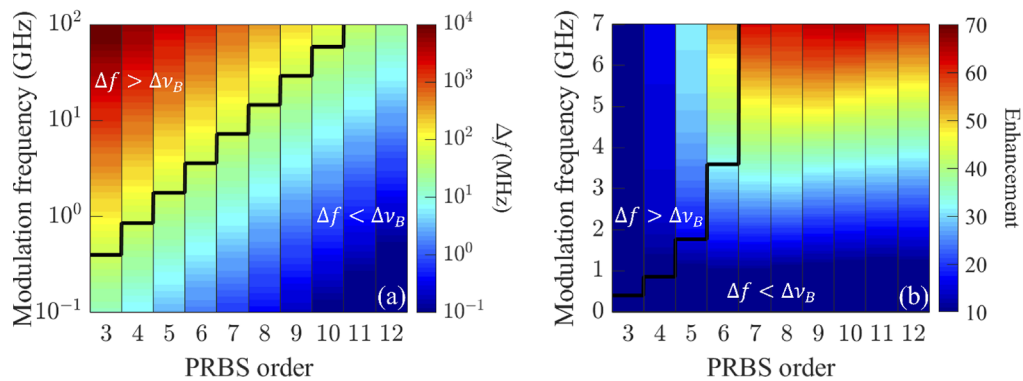

Fig. 6. (a) Tone spacing Δf and (b) enhancement as a function of modulation frequency and PRBS order.

Furthermore, Fig. 6(b) shows that using too large a PRBS order will lead to the deterioration of the enhancement rather than an improvement with a fixed modulation frequency. For example, at a modulation frequency of 3 GHz, the optimal PRBS order is 8. In addition, at a larger modulation frequency of 5 GHz, the optimal PRBS order is 9. As the modulation frequency increases, the optimal PRBS order also increases.

5. Enhancement as averaging time changes

Most prior studies of the power threshold for BI have defined the power threshold as the power at which the reflectivity reaches 1%. One issue that may arise from this definition is that averaging the Stokes power over large time scales reduces the impact of a large transient peak power. However, the Stokes wave exhibits strong fluctuations with the peak power being many times higher than its average power [22,37,38] which can lead to device damage. Hence, we consider a new BI power threshold, where we use a moving average over the nanosecond scale, defined as when the maximum averaged reflectivity over a finite time span of τ, $P_{\text{TH}}(\tau) = \max[\int_{t}^{t+\tau} \rho_S(T)dT/\tau]$

reaches 1%, with τ representing the averaging time. This definition of power threshold that depends on the averaging time avoids the appearance in the PRBS of an unmodulated sequence that is comparable to the transient time in the fiber amplifier. We still define the enhancement as the ratio of $P_{TH}(\tau)$ to the power threshold of the unmodulated input signal. To be consistent with the previous sections, the power threshold of unmodulated input signal is still averaged over 40 transient times, so that we can directly compare the data to the previous sections. Figure 7(a) shows the enhancement as a function of PRBS order for different averaging times, τ, and for a 9-m fiber. The modulation frequency is 5 GHz. The solid blue curve in Fig. 7(a) is a slice from the enhancement contour in Fig. 6(b), where the reflectivity is averaged over 40 transient fiber times, which is 1.74 μs. The blue curve has a maximum at a PRBS order of 9. In this case, the unmodulated phase sequence has a time span of $(2^8 − 1) / 5$ GHz = 51 ns, which corresponds to transient fiber time of $t_f = 43$ ns. The enhancement decreases as the PRBS order increases to values greater than 9, and illustrates the impact of the larger transient peak power with a longer PRBS sequence. As the averaging time τ decreases, which is more sensitive to any transient reflected peak pulses due to BI, the enhancement decreases. As the averaging time, τ, further decreases, the difference in enhancement becomes small, which is because the Stokes light does not rapidly change on the sub-nanosecond time scale [37]. The time step used in simulation is 50 ps.
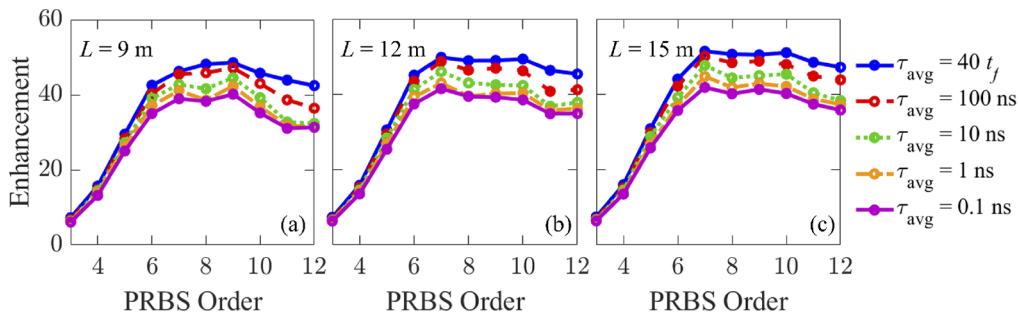
Fig. 7. Enhancement as a function of PRBS order for different averaging times and with fiber lengths of (a) 9 m, (b) 12 m, and (c) 15 m.

Next, we study the enhancement as we change the fiber length to 12 m and 15 m, as shown in Figs. 7(b) and 7(c), respectively. The enhancement becomes slightly larger because of the lower power threshold for the unmodulated case in a longer fiber. The actual power thresholds for the 12-m- and 15-m-long fibers are lower than the power thresholds for the 9-m-long fiber. This result is consistent with results from [19]. Figure 7 also shows that the enhancement saturates as the averaging time becomes either small or large.

Next, we study how the enhancement changes as the average time changes. In Fig. 8, we simulate 10 different realizations for each averaging time and plot the average enhancement for fiber lengths of 9, 12, and 15 m. Increasing the fiber length will shift the enhancement to larger values, which is consistent with Fig. 7. The modulation frequency used is 5 GHz, and the PRBS order used is 8. Figure 8 shows the saturation in the enhancement that occurs when the averaging time becomes small or large.
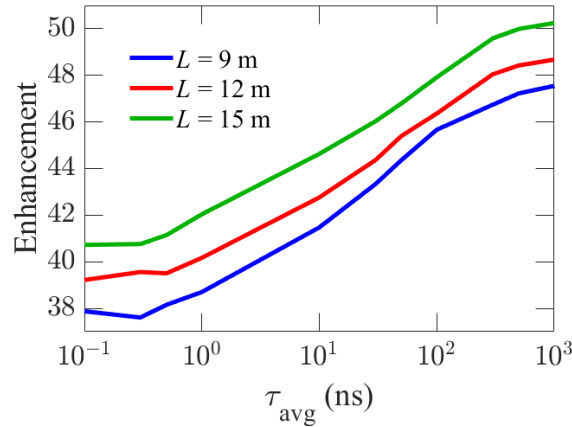
Fig. 8. Enhancement as a function of averaging times and for different fiber lengths.

## 6. Prediction of enhancement with different PRBS orders

In this section, we will derive a simple equation for the threshold power with different PRBS orders. With a fixed tone spacing Δf, the BI threshold is primarily determined by the largest power among all the different frequency tones, given the approximation that the power is almost evenly distributed near the center frequency according to Fig. 2. Hence, the largest power among all frequency tones is the same at the BI threshold with the same tone spacing Δf, but at different PRBS orders. According to Fig. 2, the laser power is mainly distributed among $2^p - 1$ and $2^q - 1$ different tones for PRBS orders of p and q, respectively. The enhancements E_p and E_q, for different orders p and q, will have a ratio $R = (2^p - 1)/(2^q - 1)$ as long as the tone spacing, Δf, is the same for those two cases. Hence, we obtain the following equation,

$$\frac{E_p(f_p) - 1}{E_q(f_q) - 1} = R, \tag{2}$$

where $E_{p,q}$ and $f_{p,q}$ are the enhancements and frequencies for PRBS orders p and q, respectively, with $f_{p,q} = \Delta f[2^{p,q} - 1]$. The numerator and denominator on the left-hand side of Eq. (2) are shifted by one because the base enhancement for all PRBS orders is one when the modulation frequency is zero. Using Eq. (2), we can predict the enhancement of order p from the enhancement of another order q by using

$$E_p(f) = R[E_q(f_p/R) - 1] + 1. \tag{3}$$

Equation (3) shows that the enhancement in the BI threshold may be predicted using the results from PRBS phase modulation with another order. Figure 9 shows the enhancement in the BI threshold as a function of modulation frequency for different PRBS orders. Black circles indicate experimental results from [22]. The solid curves are the enhancement using time dependent simulations according to Eq. (1). Dashed curves represent the enhancement using PRBS orders 5, 7, and 9, using Eq. (3) according to the solid blue curve for PRBS order 3. The dashed curves using Eq. (3) predict the trends of the corresponding solid curves from time-dependent simulations. For the solid red and dashed red curves when modulation frequency is more than 2 GHz, the value of Δf surpasses the Brillouin linewidth, and the enhancement saturates. A small discrepancy does exist between the analytical and simulation results due to the difference in the magnitude envelopes of the frequency tones in different PRBS orders, as indicated in Fig. 2. Simulations at a high PRBS order require more computation time. Equation (3) makes it possible to quickly predict the enhancement at a higher PRBS order from simulations at a lower PRBS order using a lower modulation frequency.
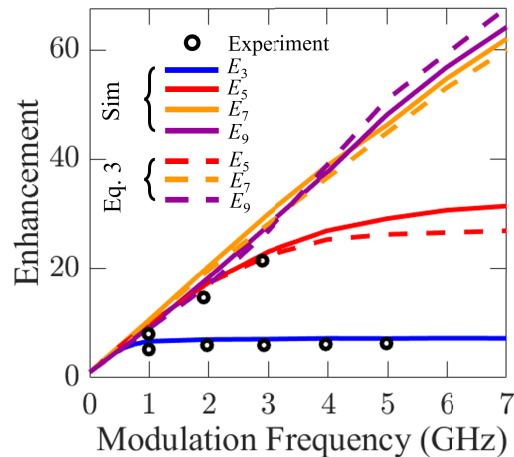
Fig. 9. Enhancement of the Brillouin instability threshold as a function of modulation frequency for different PRBS orders. Solid curves represent time dependent simulation results based on Eq. (1), and dashed curves represent the corresponding predicted enhancement based on Eq. (3). Black circles indicate experimental results from [22].

7.　Conclusions

We theoretically studied the BI threshold in a passive fiber in which the input signal is modulated using a pseudo-random bitstream (PRBS). Suppression of the Brillouin instability may be done by phase modulation that broadens the laser linewidth so that it is greater than the Brillouin bandwidth. We determined the dependence of the threshold as the Brillouin linewidth and the PRBS order varies at a fixed modulation frequency. PRBS phase modulation with a higher order will separate the modulation power into a larger number of frequency tones with a lower power, leading to a higher enhancement of the Brillouin threshold relative to the unmodulated threshold. However, the enhancement will reach saturation when the tone spacing becomes equal to the Brillouin bandwidth. Our work finds the minimum PRBS order for a specific power and Brillouin linewidth. When a specific threshold power is desired, the minimum PRBS order required decreases as the Brillouin linewidth increases. Our analysis has elucidated the relationship between the optimal PRBS order, power threshold, and Brillouin linewidth, which is important to understand the fundamental limit when designing high-power lasers. We also investigated the dependence of the optimal PRBS order on the averaging time and fiber length, and we did not find a significant dependence. Finally, we showed that it is possible to predict the enhancement achieved from a higher order PRBS pattern using a lower order PRBS pattern, which provides a computationally time-efficient method to calculate the enhancement.

Disclosures.　The authors declare no conflicts of interest.

Data availability.　Data underlying the results presented in this paper are not publicly available at this time but may be obtained from the authors upon reasonable request.

References

1. D. J. Richardson, J. Nilsson, and W. A. Clarkson, "High power fiber lasers: current status and future perspectives [Invited]," J. Opt. Soc. Am. B **27**(11), B63–B92 (2010).
2. C. Jauregui, J. Limpert, and A. Tünnermann, "High-power fibre lasers," Nat. Photonics **7**(11), 861–867 (2013).

3. M. N. Zervas and C. A. Codemard, "High power fiber lasers: a review," IEEE J. Quantum Electron. **20**(5), 219–241 (2014).
4. C. E. Mungan, S. D. Rogers, N. Satyan, and J. O. White, "Time-dependent modeling of Brillouin scattering in optical fibers excited by a chirped diode laser," IEEE J. Quantum Electron. **48**(12), 1542–1546 (2012).
5. R. W. Boyd, *Nonlinear Optics*, 2nd ed. (Academic Press, 2003) Chap. 9.
6. A Kobyakov, M Sauer, and D Chowdhury, "Stimulated Brillouin scattering in optical fibers," Adv. Opt. Photonics **2**(1), 1–59 (2010).
7. J. T. Young, A. J. Goers, D. M. Brown, M. L. Dennis, K. Lehr, C. Wei, C. R. Menyuk, and J. Hu, "Tradeoff Between the Brillouin and Transverse Mode Instabilities in Yb-doped Fiber Amplifiers," Opt. Express **30**(22), 40691–40703 (2022).
8. S. Naderi, I. Dajani, T. Madden, and C. Robin, "Investigations of modal instabilities in fiber amplifiers through detailed numerical simulations," Opt. Express **21**(13), 16111–16129 (2013).
9. A. V. Smith and J. J. Smith, "Mode instability in high power fiber amplifiers," Opt. Express **19**(11), 10180–10192 (2011).
10. K. R. Hansen, T. T. Alkeskjold, J. Broeng, and J. Laegsgaard, "Theoretical analysis of mode instability in high-power fiber amplifiers," Opt. Express **21**(2), 1944–1971 (2013).
11. C. R. Menyuk, J. T. Young, J. Hu, A. J. Goers, D. M. Brown, and M. L. Dennis, "Accurate and efficient modeling of the transverse mode instability in high energy laser amplifiers," Opt. Express **29**(12), 17746–17757 (2021).
12. C. Jauregui, C. Stihler, and J. Limpert, "Transverse mode instability," Adv. Opt. Photonics **12**(2), 429–484 (2020).
13. H.-J. Otto, F. Stutzki, F. Jansen, T. Eidam, C. Jauregui, J. Limpert, and A. Tünnermann, "Temporal dynamics of mode instabilities in high-power fiber lasers and amplifiers," Opt. Express **20**(14), 15710–15722 (2012).
14. M.-J. Li, X. Chen, J. Wang, S. Gray, A. Liu, J. A. Demeritt, A. B. Ruffin, A. M. Crowley, D. T. Walton, and L. A. Zenteno, "Al/Ge co-doped large mode area fiber with high SBS threshold," Opt. Express **15**(13), 8290–8299 (2007).
15. C Zeringue, C Vergien, and I Dajani, "Pump-limited, 203 W, single-frequency monolithic fiber amplifier based on laser gain competition," Opt. Lett. **36**(5), 618–620 (2011).
16. B. M. Cannon, D. M.. Brown, M. J. Mayr, M. L. Dennis, W. E. Torruellas, and J. O. White, "High energy fiber laser amplifier with reduced optical linewidth," US patent 20180269645A1 (Sep. 20, 2018).
17. D. Brown, M. Dennis, and W. Torruellas, "Improved phase modulation for SBS mitigation in kW-class fiber amplifiers," presented at the SPIE Photon. West, San Francisco, CA, USA, Jan. 2011.
18. A. V. Harish and J. Nilsson, "Optimization of phase modulation formats for suppression of stimulated Brillouin scattering in optical fibers," IEEE J. Quantum Electron. **24**(3), 1–10 (2018).
19. C. Zeringue, I. Dajani, S. Naderi, G. T. Moore, and C. Robin, "A theoretical study of transient stimulated Brillouin scattering in optical fibers seeded with phase-modulated light," Opt. Express **20**(19), 21196–21213 (2012).
20. B. Anderson, A. Flores, R. Holten, and I. Dajani, "Comparison of phase modulation schemes for coherently combined fiber amplifiers," Opt. Express **23**(21), 27046–27060 (2015).
21. J. B. Coles, B. P.-P. Kuo, N. Alic, S. Moro, C.-S. Bres, J. M. Chavez Boggio, P. A. Andrekson, M. Karlsson, and S. Radic, "Bandwidth-efficient phase modulation techniques for stimulated Brillouin scattering suppression in fiber optic parametric amplifiers," Opt. Express **18**(17), 18138–18150 (2010).
22. A. Flores, C. Robin, A. Lanari, and I. Dajani, "Pseudo-random binary sequence phase modulation for narrow linewidth, kilowatt, monolithic fiber amplifiers," Opt. Express **22**(15), 17735–17744 (2014).
23. N. A. Naderi, A. Flores, B. M. Anderson, and I. Dajani, "Beam combinable, kilowatt, all-fiber amplifier based on phase-modulated laser gain competition," Opt. Lett. **41**(17), 3964–3967 (2016).
24. J. O. White, A. Vasilyev, J. P. Cahill, N. Satyan, O. Okusaga, G. Rakuljic, C. E. Mungan, and A. Yariv, "Suppression of stimulated Brillouin scattering in optical fibers using a linearly chirped diode laser," Opt. Express **20**(14), 15872–15881 (2012).
25. L.-G. Hwa, J. Schroeder, and X.-S. Zhao, "Intrinsic Brillouin linewidths and stimulated Brillouin gain coefficients in glasses studied by inelastic light scattering," J. Opt. Soc. Am. B **6**(4), 833–839 (1989).
26. G. W. Faris, L. E. Jusinski, and A. P. Hickman, "High-resolution stimulated Brillouin gain spectroscopy in glasses and crystals," J. Opt. Soc. Am. B **10**(4), 587–599 (1993).
27. E. P. Ippen and R. H. Stolen, "Stimulated Brillouin scattering in optical fibers," Appl. Phys. Lett. **21**(11), 539–541 (1972).
28. J. O. White, J. T. Young, C. Wei, J. Hu, and C. R. Menyuk, "Seeding fiber amplifiers with piecewise parabolic phase modulation for high SBS thresholds and compact spectra," Opt. Express **27**(3), 2962–2974 (2019).
29. C. Wang, M. Zhang, X. Chen, M. Bertrand, A. Shams-Ansari, S. Chandrasekhar, P. Winzer, and M. Lončar, "Integrated lithium niobate electro-optic modulators operating at CMOS-compatible voltages," Nature **562**(7725), 101–104 (2018).
30. W. Stepien and J. R. Marciante, "Impact of finite bandwidth on PRBS-modulated optical spectra," Opt. Express **30**(20), 35894–35910 (2022).
31. B. Anderson, A. Flores, and I. Dajani, "Filtered pseudo random modulated fiber amplifier with enhanced coherence and nonlinear suppression," Opt. Express **25**(15), 17671–17682 (2017).
32. S. W. Golomb, *Shift Register Sequences* (Aegean Park Press, 1967).
33. B. Li, M. Liu, Y. Yang, Y. Xian, B. He, and J. Zhou, "Effective brillouin gain spectra broadening for SBS suppression based on pseudo random bit sequence phase modulation in fiber system," IEEE Photonics J. **13**(6), 1–5 (2021).

34. Y. Yang, B. Li, M. Liu, X. Huang, Y. Feng, D. Cheng, B. He, J. Zhou, and J. Nilsson, "Optimization and visualization of phase modulation with filtered and amplified maximal-length sequence for SBS suppression in a short fiber system: a theoretical treatment," Opt. Express **29**(11), 16781–16803 (2021).

35. R. W. Boyd, K. Rzągewski, and P. Narum, "Noise initiation of stimulated Brillouin scattering," Phys. Rev. A **42**(9), 5514–5521 (1990).

36. W. H. Press, S. A. Teukolsky, W. T. Vetterling, and B. P. Flannery, *Numerical Recipes: The Art of Scientific Computing*, 3rd ed. (Cambridge University Press, 2007), Chap.18.

37. A. L. Gaeta and R. W. Boyd, "Stochastic dynamics of stimulated Brillouin scattering in an optical fiber," Phys. Rev. A **44**(5), 3205–3209 (1991).

38. A. Hook and A. Bolle, "Transient Dynamics of Stimulated Brillouin Scattering in Optical Communication Systems," J. Lightwave Technol. **10**(4), 493–502 (1992).